Continental Shelf Research 234 (2022) 104642

Contents lists available at ScienceDirect

Continental Shelf Research

journal homepage: www.elsevier.com/locate/csr

Tidal change in response to the relative sea level rise and marsh accretion in a tidally choked estuary

Ali Reza Payandeh [a,*], Dubravko Justic [a], Haosheng Huang [a], Giulio Mariotti [a,b], Scott C. Hagen [b]

[a] Department of Oceanography and Coastal Sciences, College of the Coast and Environment, Louisiana State University, Iran
[b] Department of Civil & Environmental Engineering, Center for Computation & Technology, Louisiana State University, Iran

ARTICLE INFO

Keywords:
Sea level rise
Marsh accretion
Tidal choking
FVCOM
Barataria Bay
Shallow estuary

ABSTRACT

Tidal range is a key factor for flooding, mixing, and transport in estuaries. Sea level rise is expected to change tidal range in the future. This change is complex, and has been showed to either increase or decrease, and vary along the estuary axis. Large changes are expected to occur in costal Louisiana, as it is experiencing some of the highest relative sea level rise (RSLR) rates in the continental USA (0.92 cm yr^{-1}). A finite volume community ocean model was used to investigate how tidal dynamics in Barataria Bay estuary will be affected by future RSLR and marsh accretion scenarios. Under the present sea level condition, five major tidal choking areas – where tidal range reduces sharply, and phase lags develops – were identified. RSLR reduced tidal choking intensity and thus increased tidal range within the estuary. Contrary to previous modeling analyses in other estuaries suggesting that flooding of the low-lying land with sea level rise would increase frictional effects and thus reduce tidal range, this study suggested that tidal range in a choked tidal system like Barataria Bay increases even when accompanied by extensive land inundation. This occurs because the channel conveyance effects are larger than the frictional effects of the low-lying areas. In the lower and the middle bay, the largest increase in tidal range occurred when the marsh area was assumed to keep pace with RSLR. Under this condition, mean tidal range could increase by a maximum of 16 cm compared to the present-day sea level condition. However, in the upper bay the largest increase in tidal range occurred when no accretion was assumed. Under this condition, mean tidal range could increase by a maximum of 13 cm. RSLR also induced amplification of tides at the head of the estuary. A detailed momentum balance analysis indicated that sea level rise shifts tidal wave regime from a dissipative tidal wave to a progressive wave, which is more susceptible to tidal amplification.

1. Introduction

Tidal range is arguably the most important parameter determining the hydrodynamics of estuaries and coastal embayments. Accelerated sea level rise has the potential to affect tidal range because sea level rise changes coastline morphology, increases water depth, and floods low-lying land areas, thereby changing the balance between the bottom friction and other forces. Changes in tides may have important implications for ecosystem dynamics in estuaries. For instance, tidal prism will be affected by changes in tidal range and, hence, the flushing capacity and residence time of an estuary will be affected as well (Du et al., 2018; Monsen et al., 2002). Additionally, tidal range changes are often associated with shifts in sediment transport, salinity intrusion, and ecosystem properties (Talke and Jay, 2020).

Tidal range response to sea level rise is complex, and has been shown to either increase or decrease, and vary along the estuary axis. Multiple modeling studies have examined this response. For example, Hagen and Bacopoulos (2012) compared the static versus dynamic response of tides to sea level rise and reported that changes in astronomic tides should be assessed as a dynamic process and not as a static one. Passeri et al. (2015a) evaluated the combined effects of historic sea level rise and morphology changes on tidal hydrodynamics in Grand Bay, Mississippi. They demonstrated that tidal amplitudes significantly increased in the semi-enclosed regions; however changes within the sound were minimal due to the open exposed shoreline. Lee et al. (2017) developed a numerical model to investigate how sea level rise may impact tides in Chesapeake Bay and Delaware Bay. They reported similar responses in both estuaries and found that when the low-lying land is prevented from flooding, tidal range increases and when it is allowed to become permanently inundated by higher sea level, tidal range decreases.

* Corresponding author.
E-mail address: alirezapayande@gmail.com (A.R. Payandeh).

https://doi.org/10.1016/j.csr.2021.104642
Received 27 July 2021; Received in revised form 10 December 2021; Accepted 29 December 2021
Available online 5 January 2022

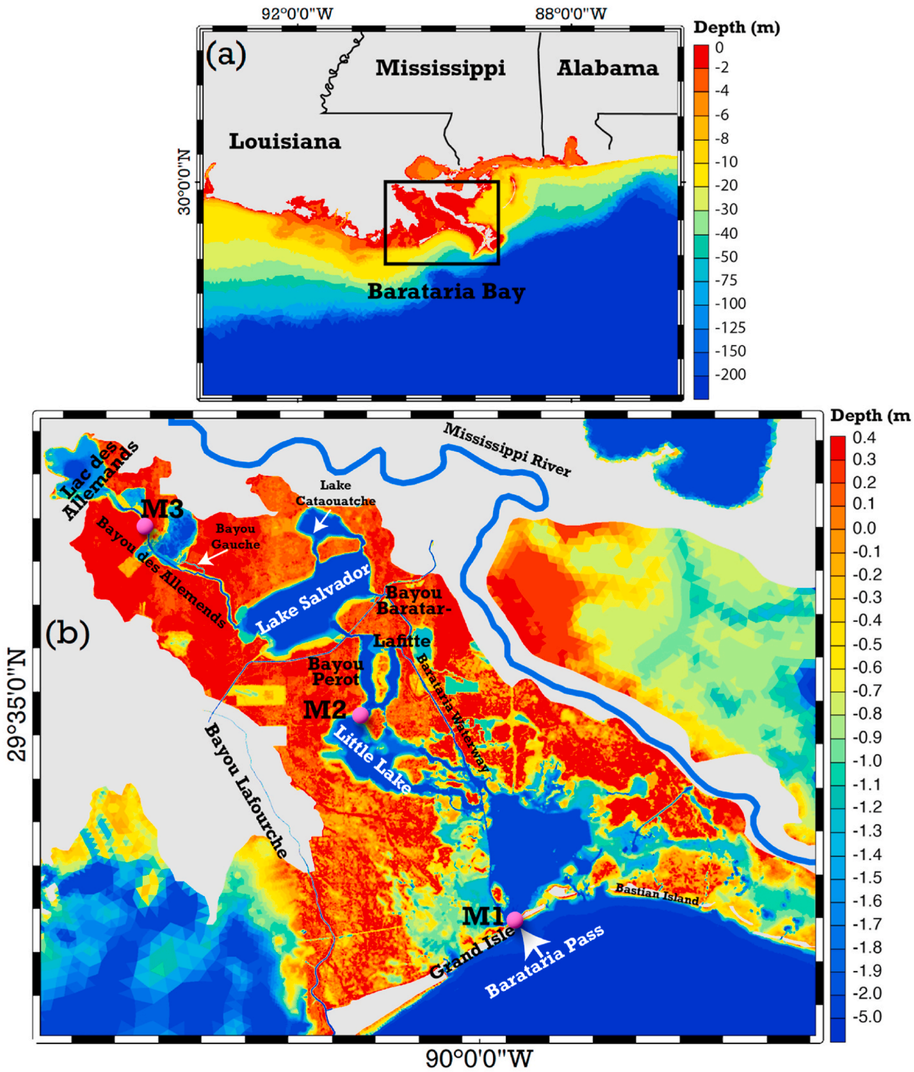

Fig. 1. The map of the (a) the northern Gulf of Mexico, and (b) Barataria Bay showing bathymetry and location of the stations used in momentum balance analysis (M1, M2, and M3).

Likewise, Holleman and Stacey (2014) implemented a numerical model to study tidal changes in San Francisco Bay under future sea level rise scenarios. They found that inundation of low-lying areas creates frictional regions that serves as energy sinks for tides, thus decreasing the tidal range under higher sea levels. Despite these similarities, tidal response to sea level rise varies among different estuaries depending on the estuarine characteristics. Du et al. (2018) found that tidal range changes under sea level rise scenarios are heavily dependent on an estuary's length and bathymetry. They showed that estuaries with a narrow channel and large low-lying areas are likely to experience decreased tidal ranges under higher sea levels. Tides increase in differently in various bays in the northern Gulf of Mexico for different sea level rise scenarios in ways as related to the projected change in inlet area (Passeri et al., 2016). Talke and Jay (2020) identified two types of systems that are prone to tidal amplification: (1) shallow, strongly damped systems, in which a small increase in water depth induces a large decrease in friction, and (2) systems in which wave reflection and resonance are strongly influenced by changes in depth, convergence and friction.

Tidal response to sea level rise is also sensitive to morphological changes (Bilskie et al., 2014; Passeri et al., 2015a). However, due to uncertainties in predicting the future geomorphology, standard approaches to exploring the impacts of sea level rise on tidal dynamics do not consider changes in geomorphology (e.g., Holleman and Stacey, 2014; Lee et al., 2017). Passeri et al. (2016) used a numerical model coupled with a probabilistic model that projects shoreline change and dune heights under future sea level rise conditions to examine the combined effects of sea level rise and morphology changes on tidal hydrodynamics along the northern Gulf of Mexico. Changes in tidal range may also affect the stability of coastal marshlands as it determines the ability to transfer sediment to the marsh platform and thus to accrete (Kirwan and Brad Murray, 2007). In addition to sediment transport processes, the ability of marshes to maintain their position depends on tidal range (Friedrichs and Perry, 2001; Torres et al., 2006). Tidal range regulates the frequency and duration of tidal inundation and thus affects rates of mineral sediment deposition on marshes (Pasternack et al., 2000). Typically, coastal marshes have kept their elevation under historic rates of sea level rise (Redfield, 1972). However, in recent decades, their ability to survive with more rapid rates of sea level rise has been questioned (e.g., Orson et al., 1985; Reed, 1995; FitzGerald et al., 2021). Using moderate sea-level rise predictions, FitzGerald et al. (2021) showed that large portions of the Great Marsh in New England are likely to be converted to low marsh by 2050, and that the entire marsh high platform will become low marsh prior to 2070. A low rate of sea level rise reduces the depth of the tidal flat, which in turn increases wave dissipation. Consequently, sediment deposition is favored, and the

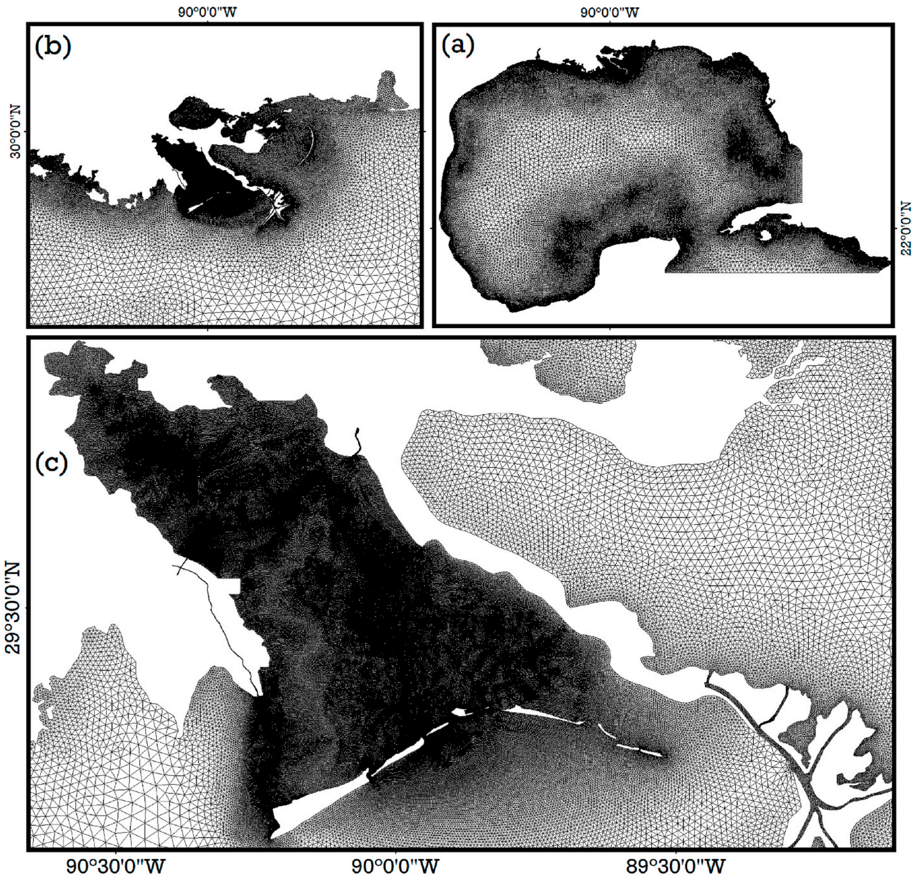

Fig. 2. Unstructured FVCOM grid for (a) entire computational domain, (b) local domain of the northern Gulf of Mexico, and (c) local domain of Barataria Bay (horizontal resolution of ~15 m).

marsh boundary prograde. In contrast, A high rate of sea level rise leads to a deeper tidal flat and thus higher waves that erode the marsh boundary, leading to erosion. When the rate of sea level rise is too fast the entire marsh drowns and is transformed into a tidal flat (Mariotti and Fagherazzi, 2010). Accordingly, in numerical modeling studies, it is important to update the morphology based on the future sea level rise projections.

Coastal Louisiana is experiencing some of the highest sea level rise rates in the US, and thus is appropriate for examining the impacts of sea level rise on estuarine tidal dynamics. In recent decades, this region has experienced globally high rates of land loss resulting from a number of anthropogenic and natural factors (Day et al., 2000, 2007; Paola et al., 2011; Hiatt et al., 2019). Many studies point to the eustatic (or global) sea level rise (ESLR) and subsidence as a major driver of land loss. The sum of ESLR and subsidence is typically referred to as relative sea-level rise (RSLR).

The total land area lost in Mississippi River delta over the last 100 years has been approximately 5000 km^2 at rates as high as 100 km^2 yr^{-1} (Day et al., 2000; Couvillion et al., 2017). Here we focus on Barataria Bay (also referred to as Barataria Estuary), which is situated between the main stem of the Mississippi River and Bayou Lafourche (Fig. 1). Barataria Bay has unique features that distinguish it from other estuaries studied before. For example, Barataria Bay is a very shallow estuary (averaged depth ~ 2 m) and has a complex geomorphology due to the presence of many lakes, bayous, channels, tidally influenced marshes and barrier islands on the south that separate the estuary from the Gulf of Mexico. There are large regions of freshwater, brackish, and saline marshes that account for more than 60% of total area of the estuary. These low-lying wetlands and marshes are prone to flooding when sea level rises. Tides in Barataria Bay are microtidal, with K1 and O1 being the dominant tidal constituents, whose amplitudes in Barataria Pass are about 15 cm. Barataria Bay is a tidally choked system and dissipates tides heavily so that they are attenuated by 68% at Lafitte located at the middle of the estuary (Fig. 1; Byrne et al., 1976; Conner et al., 1987). The combined effects of RSLR and potentially increasing tidal ranges will have pervasive effects on Barataria Bay. Thus, as sea level rises, it is imperative to quantify how tidal dynamics in this estuary will be affected by RSLR. In order to have a thorough understanding of the tidal and tidal components' responses to future RSLR and marsh accretion in Barataria Bay, a comprehensive modeling study is conducted. Spatial variations of tides and tidal components between present-day scenario and RSLR scenarios are examined.

2. Methodology

A numerical model was developed to explore the effects of RSLR and marsh accretion on tidal dynamics in Barataria Bay. Different model scenarios were employed to simulate tides under various future RSLR and marsh accretion conditions. The changes in the tidal dynamics were explored through an analysis of the momentum equations.

3. Model setup

In this study, the Finite Volume Community Ocean Model (FVCOM) was used to examine the effects of RSLR on tidal dynamics. FVCOM solves the governing equations using an unstructured grid (Chen et al., 2003, 2013). It has been used successfully in many studies around the world including studies of the northern Gulf of Mexico (Huang et al., 2011; Huang and Li, 2017; Li et al., 2011; Payandeh et al., 2019; Wang and Justic, 2009). The system of governing equations consists of the

Table 1
Values used in the nine future RSLR scenarios for the next 50 years (RSLR = ESLR + Subsidence). Subsidence ranges were derived from a map of plausible subsidence rates for coastal Louisiana, separated into 17 geographical regions (CPRA, 2012- Appendix C).

Scenario	ESLR (m/50 yr)	Subsidence (m/50 yr)	Accretion rate of marsh (m/50 yr)
Lowest1	0.43	20% of range	without accretion
Lowest2	0.43	20% of range	50% of RSLR
Lowest3	0.43	20% of range	100% of RSLR
Medium1	0.63	20% of range	without accretion
Medium2	0.63	20% of range	50% of RSLR
Medium3	0.63	20% of range	100% of RSLR
Highest1	0.83	50% of range	without accretion
Highest2	0.83	50% of range	50% of RSLR
Highest3	0.83	50% of range	100% of RSLR

Table 2
List of 30 stations used in the model-observation comparisons.

State	Station ID	NOAA/USGS ID	Station location
TX	SLR01	8,775,270	Port Aransas
TX	SLR02	8,772,471	Freeport Harbor
LA	SLR03	8,768,094	Calcasieu Pass
LA	SLR04	8,763,535	Caillou Bay
LA	SLR05	8,762,888	Lake Pelto
LA	SLR06	8,762,223	Timbalier Bay
LA	SLR07	8,761,724	Grand Isle
LA	SLR08	291,929,089,562,600	Grand Terre Island
LA	SLR09	8,761,742	Mendicant Island
LA	SLR10	8,761,819	Hackberry Bay
LA	SLR11	292,859,090,004,000	S of Lafitte
LA	SLR12	292,800,090,060,000	Bay Dosgris
LA	SLR13	07,380,335	Little Lake
LA	SLR14	07,380,330	Bayou Perot
LA	SLR15	2,951,190,901,217	Lake Cataouatche
LA	SLR16	8,762,482	Bayou Gauche
LA	SLR17	8,760,943	SW Pass
LA	SLR18	8,760,551	South Pass
LA	SLR19	8,760,417	Devon Energy Facility
LA	SLR20	8,760,668	Grand Pass
MS	SLR21	747,437	Bay Waveland
AL	SLR22	8,735,180	Dauphin Island
FL	SLR23	8,729,678	Navarre Beach
FL	SLR24	8,729,210	Panama City Beach
FL	SLR25	8,726,347	Egmont Key
FL	SLR26	8,726,724	Clearwater Beach
FL	SLR27	8,725,110	Naples
FL	SLR28	8,724,967	Marco Island
FL	SLR29	8,724,580	Key West
FL	SLR30	8,724,698	Loggerhead Key

momentum, continuity, temperature, salinity, and density equations under the Boussinesq and hydrostatic approximations. The detailed formulations and numerical aspects of FVCOM can be found in Chen et al. (2013) and they will not be repeated here.

Sea level rise could change tidal amplitudes in the open ocean and over the continental shelf (Pickering et al., 2012, 2017). Therefore, FVCOM was implemented to the entire Gulf of Mexico with a focus on the northern Gulf of Mexico and particularly Barataria Bay for which a high spatial resolution (~15 m) was implemented. As shown in Fig. 2, the model domain covers all the lakes, bayous, channels and major waterways along the estuary. The numerical mesh consists of 700,224 cells and 356,816 nodes. Bathymetric data were obtained from Coastal Louisiana Ecosystem Assessment and Restoration Report (CLEAR), and Digital Elevation Models (DEM) developed by NOAA's National Geophysical Data Center (NGDC) with 10 m resolution and were interpolated to the grid using an inverse distance weighted method. The model has two open boundaries as shown in Fig. 2: (i) a latitudinal line in the northern Caribbean Sea and (ii) the Strait of Florida. The tidal forcing was implemented by specifying the amplitudes and phases of eight dominant astronomic tides (S_2, M_2, N_2, K_2, K_1, O_1, P_1, and Q_1) at model open boundaries, derived from ADCIRC EC2015 tidal databases (Szpilka et al., 2016). Tidal potential forcing was also applied for the Gulf of Mexico using the same eight tidal constituents. The flooding and drying treatment was implemented by taking into account the water level fluctuations over intertidal zone and allowing the flooding of low-lying areas beyond the present shorelines as sea level rises. All simulations began with a null state and were run for 100 days. The first 20 days were model spin-up period, over which all forcings were ramped up from zero to their full values. Thus, all harmonics were analyzed during the last 80 days of the simulations. Future sea level rise scenarios were implemented in the model by adding an additional steady component to open boundaries. This component had a zero-phase and an amplitude equal to the ESLR for the given scenario. In addition, for each scenario, bathymetry was updated to represent the subsidence and marsh accretion under future conditions. Changes in tidal range were quantified by calculating the Mean Tidal Range (MTR) as well as the amplitude of individual harmonics such as K_1 and O_1. MTR was calculated as: mean high water (MHW) - mean low water (MLW). MTR difference was also calculated as the MTR for a specific scenario minus MTR under the present-day sea level condition.

4. Model experiments

Siverd et al. (2019) demonstrated the need to take into account ESLR and subsidence (i.e., RSLR) when examining future hydrodynamic responses on the Louisiana coastal land margins. A numerical modeling study by Blum et al. (2008) suggested subsidence rates of approximately 1 mm yr^{-1} produced by lithospheric flexure. Veatch (2015) reported a relatively long time series (~50 years) of RSLR values derived from 19 tide gauges along the Louisiana Coast. They reported a RSLR rate of 10.8, 7.0, and 11.75 mm yr^{-1} for Bayou Lafourche, Bayou Barataria, and West Pointe a la Hache respectively. Hence, subsidence rates are spatially different, presenting a challenge in defining estimates for the future RSLR scenarios. In this study, nine distinct RSLR scenarios representative for the next 50 years were categorized into three major classes of Lowest, Medium and Highest. Subsidence and ESLR for each scenario were defined following a similar approach used in the 2012 Coastal Master Plan (CPRA, 2012). CPRA provides ESLR and subsidence rates for three possible scenarios (i.e., Lowest, Medium and Highest) for the next 50 years. These rates as well as marsh accretion rates considered in this study are shown in Table 1. Subsidence rates defined by CPRA for the Lowest, Medium and Highest scenarios are 20%, 20% and 50% of the plausible subsidence rates respectively. Subsidence ranges were derived from a map of plausible subsidence rates (ranging from 0 to 35 mm yr^{-1}) for coastal Louisiana, separated into 17 geographical regions (CPRA, 2012- Appendix C). For example, the lower Barataria Bay subsidence zone had a range of observed subsidence rates between 6 and 20 mm yr^{-1}, therefore, for the highest scenario, the 50th percentile value is equal to 13 mm yr^{-1} or $13 \times 50 = 650$ mm/50 years.

Incorporating coastal mechanisms to modify morphology in response to future inundation changes under RSLR and informing the model is challenging due to the lack of comprehensive models that predict accretion and erosion in response to sea level rise (Zhang, 2011; Passeri et al., 2015b). Short term accretion rates provided by Coastwide Reference Monitoring System (CRMS) shows high spatial variability in Barataria Bay ranging from 0.48 cm yr^{-1} in Bayou Wilkinson to 2.39 cm yr^{-1} in Bayou Dupont. Therefore, the range of accretion is such that some marshes keep pace with RSLR, while others are losing elevation and will eventually drown. Comparison of long-term accretion rates produced by Shrull (2018) and CRMS short term rates show that these rates are time dependent, and the period of observation can change the observed rates. Here in order to explore the effect of marsh accretion on tidal dynamics and as a first order approximation, in each group three scenarios are considered: (i) without accretion in which the marsh has no vertical accretion in response to the RSLR, (ii) an accretion rate equal

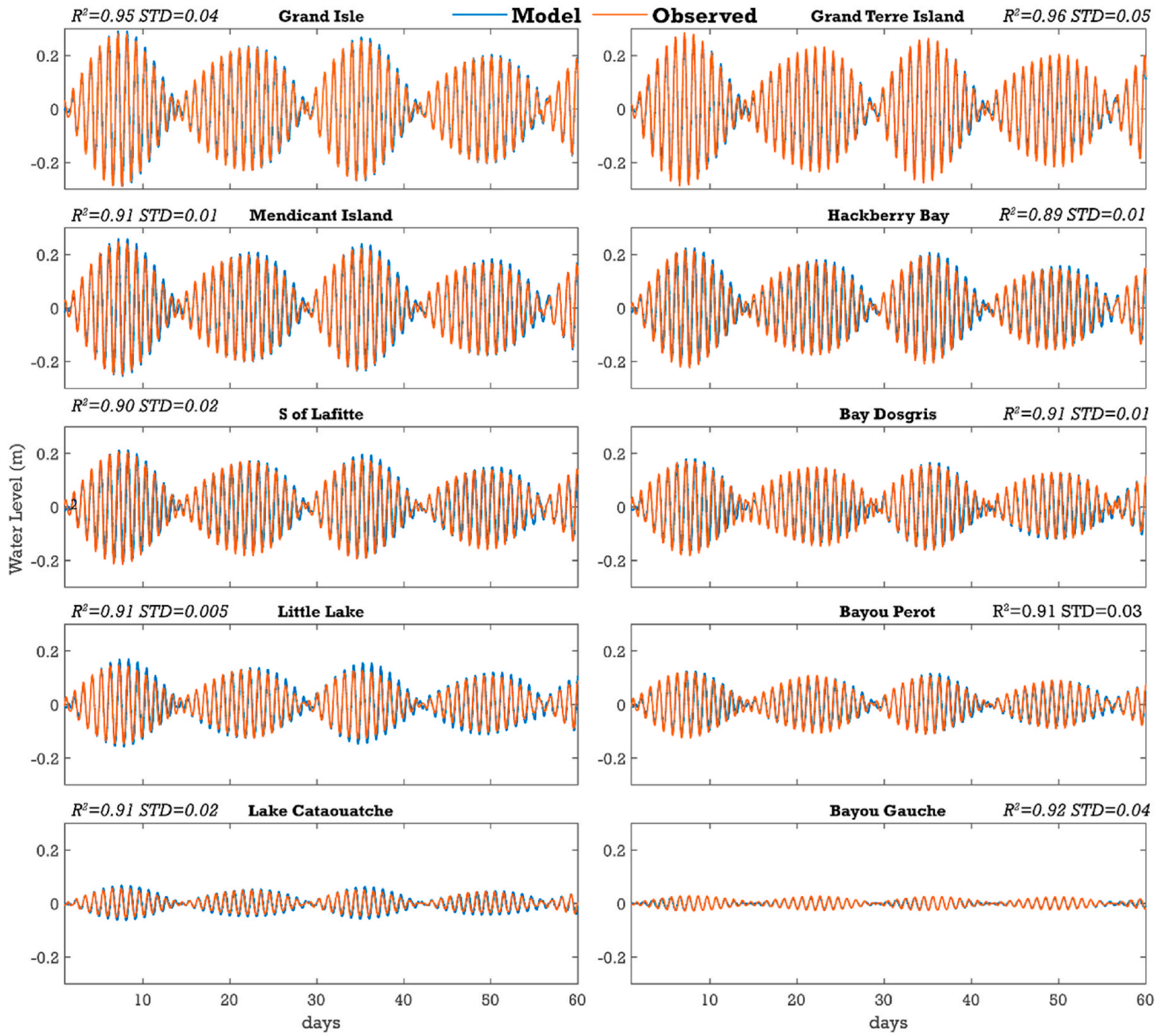

Fig. 3. Comparisons between modeled and observed tidal water levels at 10 sample stations within Barataria Bay. R^2 and STD denote correlation coefficient squared and standard deviation, respectively.

to 50% of its corresponding RSLR value and (iii) an accretion rate equal to 100% of its corresponding RSLR value, which means the marsh is able to keep pace with RSLR (Table 1). The state of Louisiana has developed a comprehensive coastal protection and restoration plan that seeks to protect all the barrier islands in the hopes of minimizing damage from future sea level rise and hurricanes to coastal communities. Accordingly, in this study we assumed that the present-day shoreline around barrier islands of the Barataria Bay will not change. This assumption is an important limitation of the model and will be discussed in Limitation of the analysis section. In model experiments flooding of extensive wetlands inside and around the estuary is allowed.

5. Error analysis

At 30 stations, the simulated 80-days water level time series were compared with the reconstructed tidal water levels, i.e., the water levels constructed by using the eight dominant harmonic constituents for each station. Amplitudes and phases of the harmonic constituents were either derived from NOAA website (https://tidesandcurrents.noaa.gov/) or calculated from observed USGS water levels. In the rest of the analysis, we will refer to the reconstructed water levels as observed water levels. In addition, tidal constituent amplitudes and phases were computed and compared at each station using two metrics. The first metric is the standard deviation (*STD*), which is calculated as the root mean square error:

$$\mathrm{STD} = \sqrt{\frac{1}{\mathrm{N}-1}\sum_{\mathrm{i}=1}^{\mathrm{N}}(\mathrm{OBS_i}-\mathrm{SIM_i})^2} \tag{1}$$

where *OBS* is the observed value and *SIM* is the simulated value. The second metric is the correlation coefficient squared (R^2) which is calculated as the square of correlation coefficient (Thomson and Emery, 2014):

$$\mathrm{R} = \frac{1}{\mathrm{N}-1}\sum_{\mathrm{i}=1}^{N}\frac{(\mathrm{OBS_i}-\overline{\mathrm{OBS}})(\mathrm{SIM_i}-\overline{\mathrm{SIM}})}{\mathrm{STD_{OBS}}\ \mathrm{STD_{SIM}}} \tag{2}$$

where $\overline{\mathrm{OBS}}$ is the mean of the observed values, $\overline{\mathrm{SIM}}$ is the mean of the simulated values, $\mathrm{STD_{OBS}}$ is the standard deviation of observed values and $\mathrm{STD_{SIM}}$ is the standard deviation of simulated values.

6. Results

6.1. Model-observation comparisons

The simulated tidal water levels for the present-day scenario were compared with the observed tidal water levels obtained from NOAA tide gauges at 30 stations. These stations are listed in Table 2 and span from

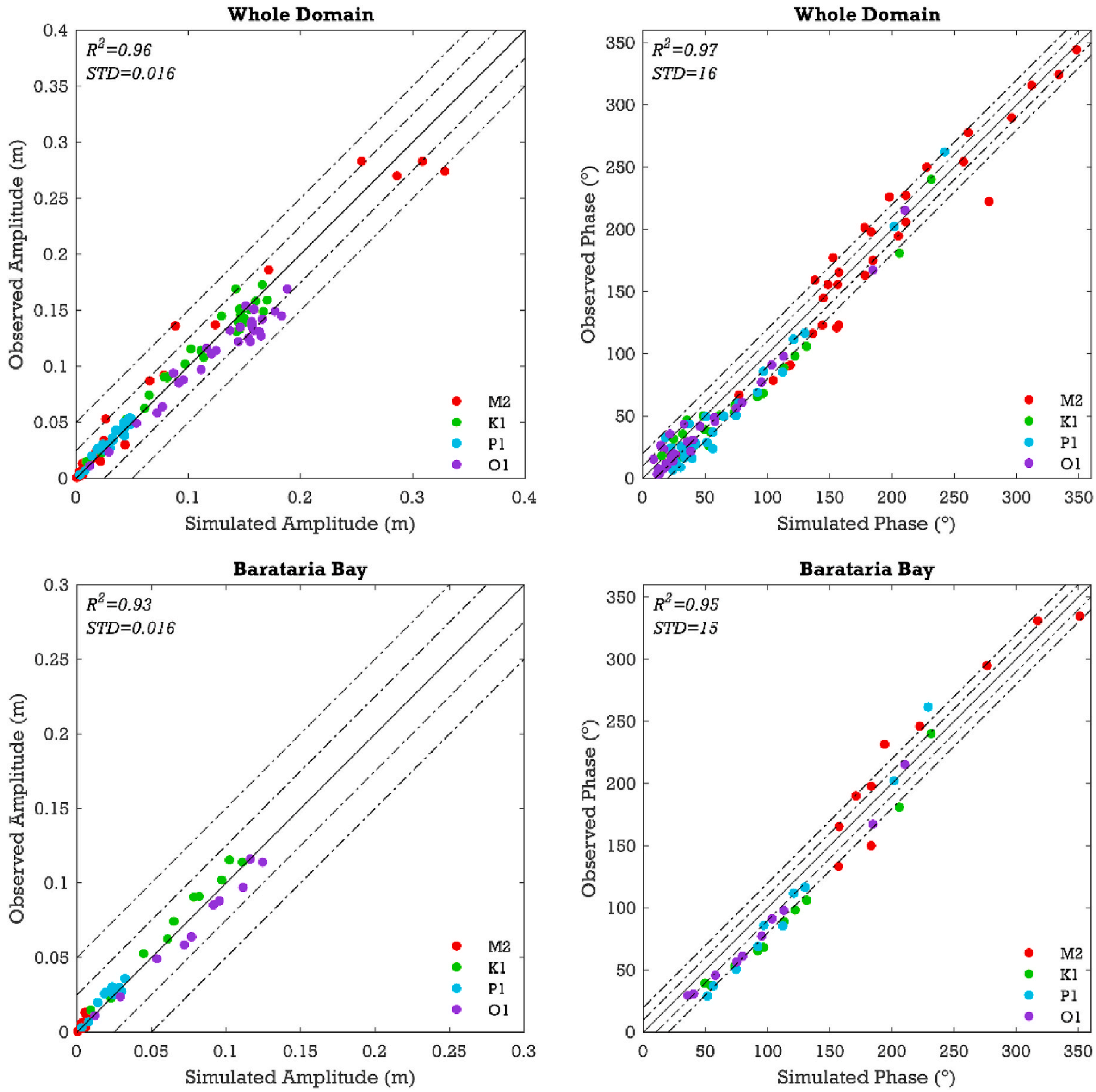

Fig. 4. Comparisons between simulated and observed tidal constituents (amplitudes and phases) for the four dominant constituents (M_2, K_1, P_1, O_1) at 30 stations. Results are separated by Barataria Bay and the entire domain. The R^2 and STD denote correlation coefficient squared and standard deviation, respectively. The error bands are defined as 0.025 and 0.05 m for the amplitude plots and 10° and 20° for the phases.

Key West in Florida to Brazos Island in Texas. Of these 30 stations, 10 are located in Barataria Bay and span from Grand Isle in the south to Bayou Gauche in the north. An example of model-observation comparisons is given in Fig. 3, which shows 60-days long time series comparisons at 10 stations inside Barataria Bay. The simulated water levels are directly extracted from the FVCOM output and the observed water levels are those constructed from the eight primary tidal constituents (S_2, M_2, N_2, K_2, K_1, P_1, O_1, Q_1). As a quantitative measure of model accuracy, the correlation coefficients squared (R^2) and standard deviation (STD) between simulated and observed water levels were computed. Overall, the simulated water levels were in good agreement with the observed water levels with R^2 ranging from 0.91 to 0.98 and the STD ranging from 0.005 to 0.05 m. Higher resolution in Barataria Bay resulted in higher accuracy in the study area where STD ranged from 0.005 to 0.02 m.

To further examine the efficiency of the model, a comparison was made between the NOAA/USGS-measured and the FVCOM-computed amplitudes and phases of tidal constituents at 30 stations. A comparison for the 4 dominant constituents (M_2, K_1, P_1, O_1) in Barataria Bay and the entire model domain, respectively is shown in Fig. 4. Different bands are defined at 0.025 and 0.05 m for the amplitude plots and 10° and 20° for the phases plots. Most of the amplitudes fall inside the 0.025 error band and others fall very near or inside the 0.05 m error band. For phases, most of the constituents fall in 10° error band and others within 20° error band. Only some phases of M_2 show significant differences. Semidiurnal constituents like M_2 are more dominant on Florida shelf up to Apalachicola. Additional resolution in this region may be required to improve the semidiurnal predictions. In addition, the NOAA measured data include measurement uncertainties due to changing bathymetry of coastal regions and nontidal events including river discharges, wind-driven events, and radiational heating cycles. These uncertainties can account for 35%–60% of the modeled to observed amplitudes and 50–80% of the phase difference (Bunya et al., 2010). Nevertheless, the results were satisfactory with R^2 of 0.94 and 0.96 for amplitudes and phases over the entire domain. For Barataria Bay, R^2 values were 0.90 and 0.96 for amplitudes and phases, respectively. The standard deviation for amplitudes was less than 0.02 m and the standard deviation for phases was less than 20° throughout the model domain. Overall, these results indicate an excellent agreement between the simulated and

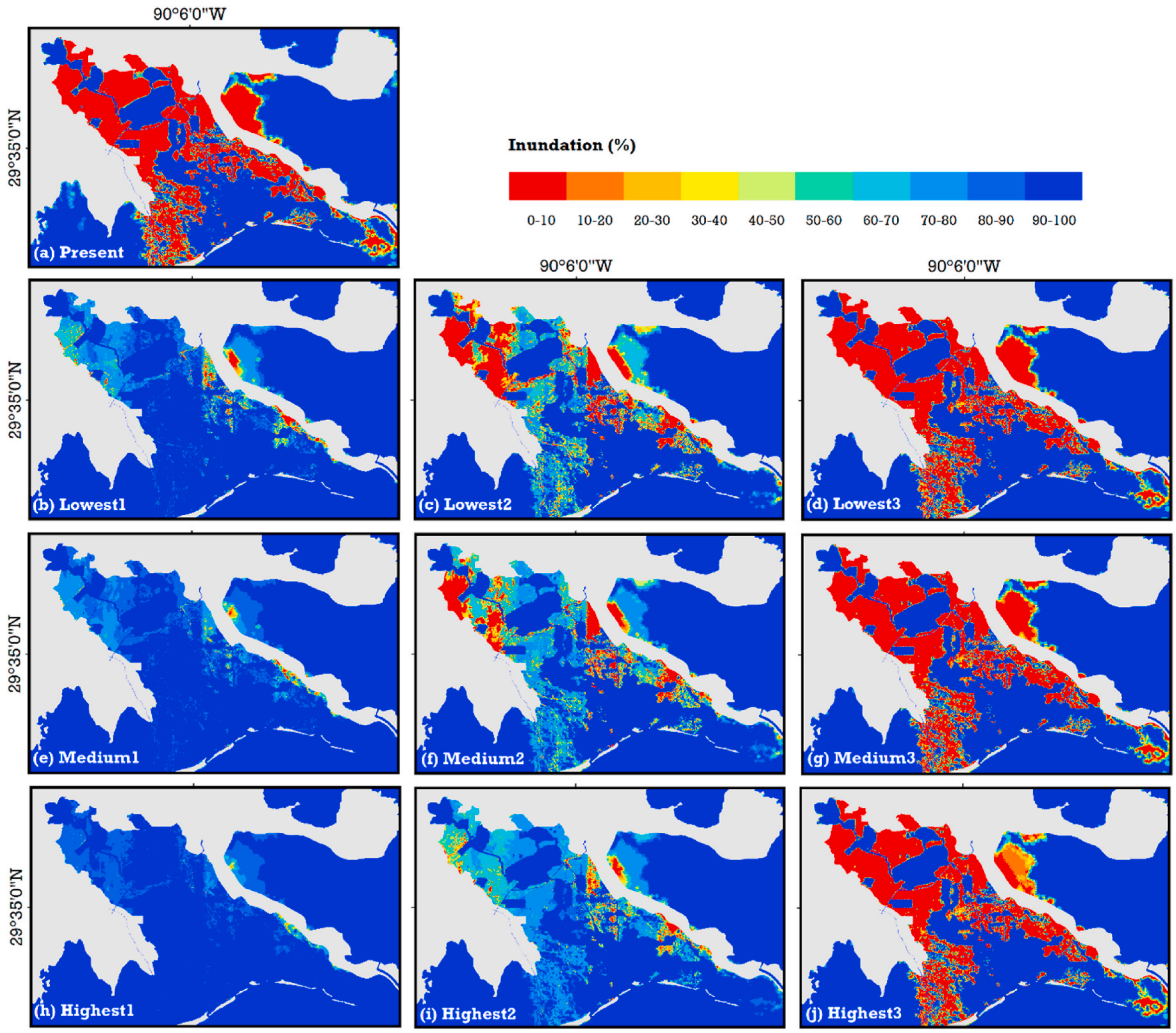

Fig. 5. Tidally induced inundation in Barataria Bay under the present-day sea level conditions and future RSLR scenarios. Inundation is shown in terms of the percent of the simulation time that a specific area is flooded, e.g., 100% means permanently flooded and 0% means never flooded.

observed amplitudes and phases.

6.2. Tidal dynamics under present sea level conditions

The extent of the flooded areas for each scenario under the present-day sea level conditions is shown in Fig. 5 and summarized in Table 3. At present, 1787 km^2, or 42%) of the total estuarine area is permanently inundated, with the estuary exhibiting complex geometry and vast intertidal areas. Although the lower estuary is relatively open, the upper estuary comprises mostly divided water bodies that are connected by small bayous and channels. Barataria Waterway, which is a relatively deep shipping channel (~4 m) that runs from the Barataria Pass along the axis of the estuary and extends to the Gulf Intracoastal Waterway, has an important role in connecting divided water bodies (Fig. 1).

K_1 and O_1 were the dominant tidal constituents, whose amplitudes on the shelf were about 15 cm (Figs. 7a and 8a). These amplitudes were constant on the shelf but sharply decreased when passing through Barataria Pass where they dropped to 9 cm just inside the bay. Five major tidal choking areas were identified within the bay represented by the vertical gray dashed lines in Fig. 7. The common feature in all of these areas was a narrow pass that connects two relatively larger water bodies within the estuary. The first tidal choking occurred in Barataria Pass where, in addition to amplitude dissipation, up to 2.5 h of phase difference also occurred (Figs. 7b and 9a). In the lower estuary, amplitudes and phases of K_1 remained relatively unchanged around 10 cm and 4 h respectively. The second tidal choking occurred when passing from the lower estuary into the Little Lake. Four small bayous connect the lower estuary to Little Lake including Bayou Saint Denis, Bayou Dosgris, Grand Bayou and Snail Bayou. The amplitude of K_1 was reduced by 3 cm in this area and the phase was lagged by 2.25 h. The third tidal choking area was located near cutoff where a small inlet connects Little Lake to Bayou Perot. Specifically, 3 cm of amplitude decay and 1.2 h of phase lag was observed at this point. Tidal dissipation continued along the Bayou Perot since it is a very shallow (~1 m) and relatively narrow body of water. The fourth major tidal choking occurred in a narrow pass connecting Bayou Perot to Lake Salvador where amplitudes were decreased by 1 cm and phases were lagged by 2.8 h. Lake Salvador is relatively deep (~3–5 m) and thus tidal amplitudes and phases remained relatively unchanged in this body of water. The last major tidal choking occurred when tides in Lake Salvador propagated into Bayou des Allemends. In this narrow bayou, amplitudes were reduced by 1.5 cm and phases were lagged by 8.2 h. In Lac des Allemands, located at the end of the model domain, K_1 amplitude was almost zero and its phase was around 21 h. Tidal phase difference between the mouth and the head of the estuary for the K_1 harmonic was 19.78 h (Table 3).

MTR was largest (33 cm) on the shelf and diminished drastically just to the north of the Barataria Pass (22 cm) (Figs. 6a and 7g). MTR was relatively constant around 22 cm in the lower bay and started diminishing again when passing from the lower estuary into the Little Lake. As expected, the MTR changes along the estuary showed the same pattern

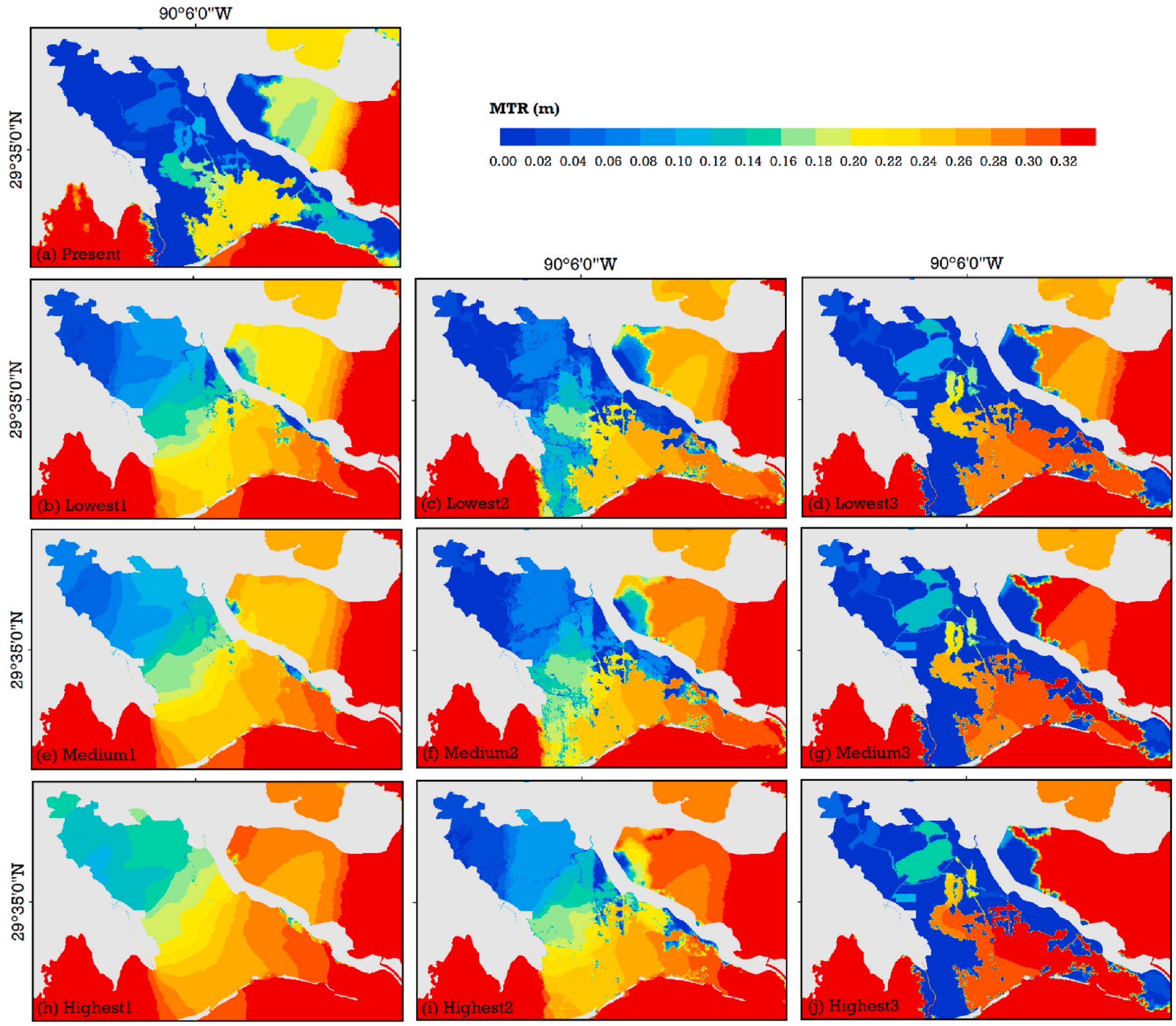

Fig. 6. Mean tidal range under the present-day sea level condition and future RSLR scenarios.

Table 3
K_1 phase difference ($\Delta\varphi$ (K_1)) and MTR difference ($\Delta\eta$) between the mouth (Barataria Pass) and the head (Lac des Allemands) of the estuary and the extent of tidally induced inundation for the present and the various RSLR scenarios.

Scenario	Δφ(K1) (hr)	Δη (m)	Area Inundated (km^2)		
			more than 99% of the simulation time	between 99 and 10% of the simulation time	less than 10% of the simulation time
Present	19.78	0.31	1787	741	1692
Lowest1	17.28	0.29	2679	1521	29
Lowest2	17.29	0.30	2023	1590	607
Lowest3	16.61	0.29	1999	575	1646
Medium1	15.12	0.25	2662	1554	4
Medium2	17.17	0.30	2000	1878	342
Medium3	16	0.28	1982	594	1644
Highest1	11.89	0.17	3206	1014	0
Highest2	17.11	0.29	2014	2149	57
Highest3	14.95	0.27	1982	608	1630

as K_1 amplitudes variations explained above. After five major tidal chokings, the MTR reached a minimum value of 2 cm in Lac des Allemands. Thus, the MTR difference between the mouth and the head of the estuary at the present sea level was 31 cm (Table 3).

7. Response to RSLR

RSLR brought negligible tidal changes on the offshore end of Barataria Bay. However, it made substantial changes to the tidal range and tidal harmonics within the estuary (Fig. 6). An overview of MTR and phase difference between the mouth and the head of the estuary as well as inundation extent in each scenario is given in Table 3. In each group of simulations (Lowest, Medium, and Highest) the most extensive inundation occurred, as expected, when no accretion was considered i. e., in the Lowest1, Medium1 and the Highest1 scenarios (Fig. 5b, e and 5h). The largest inundation among all scenarios occurred in the Highest1 which was the least optimistic scenario with the largest ESLR and subsidence and no accretion of marshes. In this scenario, 3206 km^2 of wetlands, accounting for 75% of the total estuarine area was flooded permanently (i.e., was flooded more than 99% of simulation time). The remaining 25% of the estuarine area was also partially flooded (10–99% of the simulation time). Even in the Lowest2, Medium2 and Highest2 scenarios in which marsh area was accreted by 50% of RSLR, extensive low-lying wetlands were flooded permanently (Fig. 5c, f and 5i). For example, in the Highest2 scenario 2014 km^2 was permanently flooded, which is equivalent of 48% of total estuarine area. An additional 2149 km^2 was partially flooded equivalent of 51% of total estuarine area. As expected, the extent of inundation for the Lowest3, Medium3 and Highest3 scenarios was similar to the present condition as it was assumed that marsh keeps pace with RSLR and therefore it was accreted by 100% of RSLR (Fig. 5d, g and 5j).

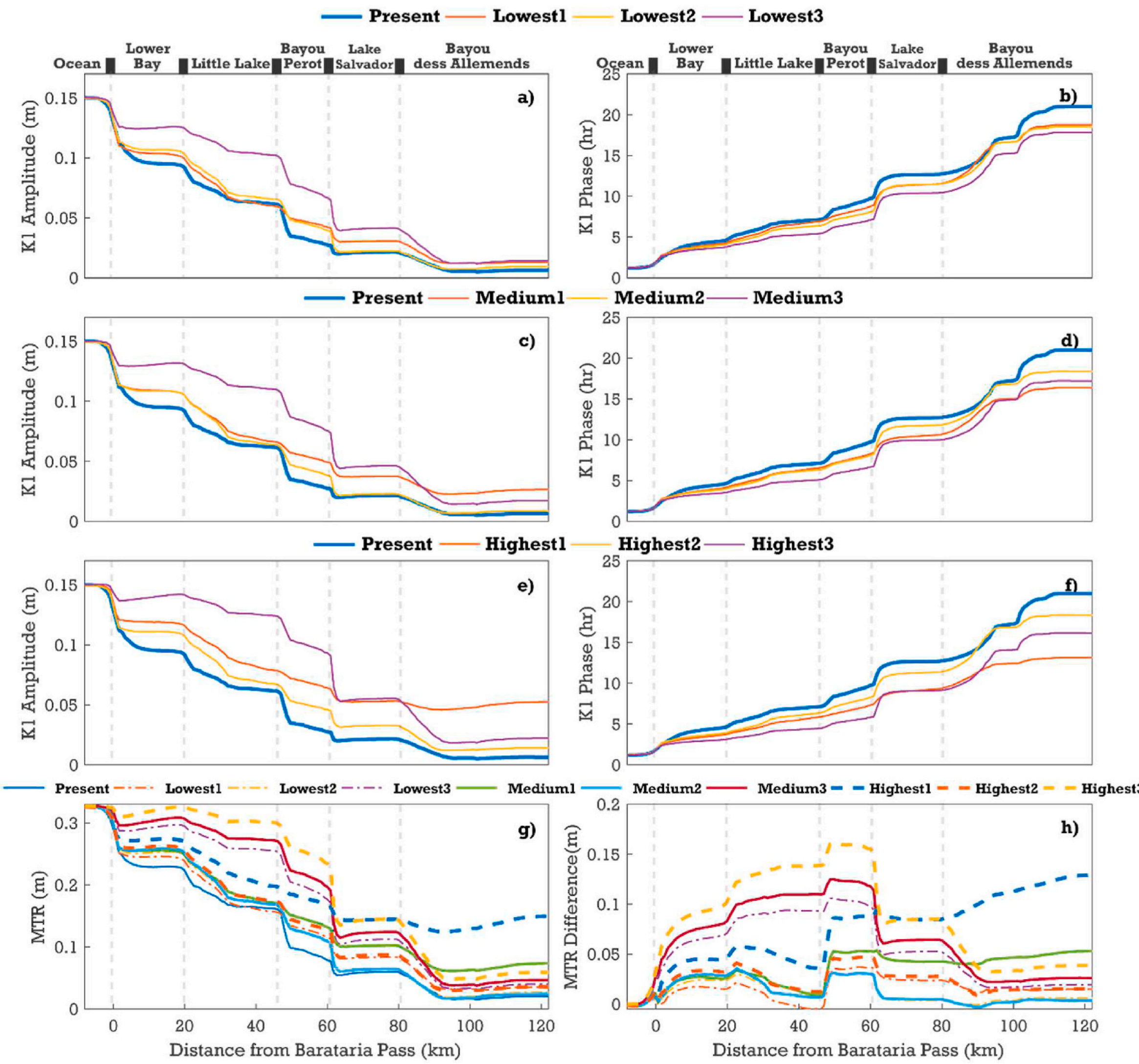

Fig. 7. Variation in K_1 amplitude, MTR and MTR difference along the estuary starting 8 km offshore of the Barataria Pass. Each vertical gray dashed line represents a narrow pass that connects larger water bodies within the estuary.

Barataria Basin experienced spatially uneven change of tidal range under RSLR and the most significant changes in each scenario occurred in newly flooded areas that remained dry in the present-day scenario but flooded under RSLR scenarios (Fig. 6). Beyond the newly flooded areas, tidal changes were smaller on the estuary's main stem that was already flooded in the present-day scenario. In these areas and in simulations with no accretion (Lowest1, Medium1 and Highest1) changes in MTR were higher at the head of the estuary compared to the lower and middle estuary regions (Fig. 6b, e, 6h). MTR under the Lowest1, Medium1 and Highest1 scenarios at the lower and middle estuary increased by a maximum of 2.0, 3.0 and 4.0 cm respectively. However, the maximum increase in MTR at the head of the estuary for the same scenarios were 3.0, 6.0 and 13 cm (Fig. 7h). In contrast, in simulations with 100% of RSLR accretion (Lowest3, Medium3, and Highest3) tidal changes in the lower and middle estuary were higher than in the upper estuary (Fig. 6d, g, 6j). MTR under the Lowest3, Medium3 and the Highest3 scenarios at the lower and middle estuary increased by a maximum of 10, 12 and 16 cm, respectively. However, MTR at the head of the estuary for those same scenarios increased by 2.0, 2.5 and 4 cm, respectively (Fig. 7h).

Tidal dissipation was the highest under the Lowest2, Medium2 and Highest2 scenarios because accretion of marsh by 50% of RSLR introduced extensive intertidal areas to the estuary that served as a sink for tidal energy. On the other hand, tidal dissipation was the lowest under the Lowest1, Medium1 and Highest1 scenarios because the flooding of low-lying areas turned the estuary into a widely open water body with significantly reduced tidal choking and frictional effects. MTR difference between the mouth and the head of the estuary clearly shows this effect. For example, the MTR difference between the mouth and the head of the estuary in the Highest2 and Highest3 were 29 and 17 cm respectively. In addition, tidal phase difference between the mouth and the head of the estuary for K_1 harmonic also reconfirmed the above-mentioned pattern. For example, phase difference between the mouth and the head of the estuary under the Highest2 and Highest3 scenarios were 17.11 h and 11.89 h respectively (Table 3).

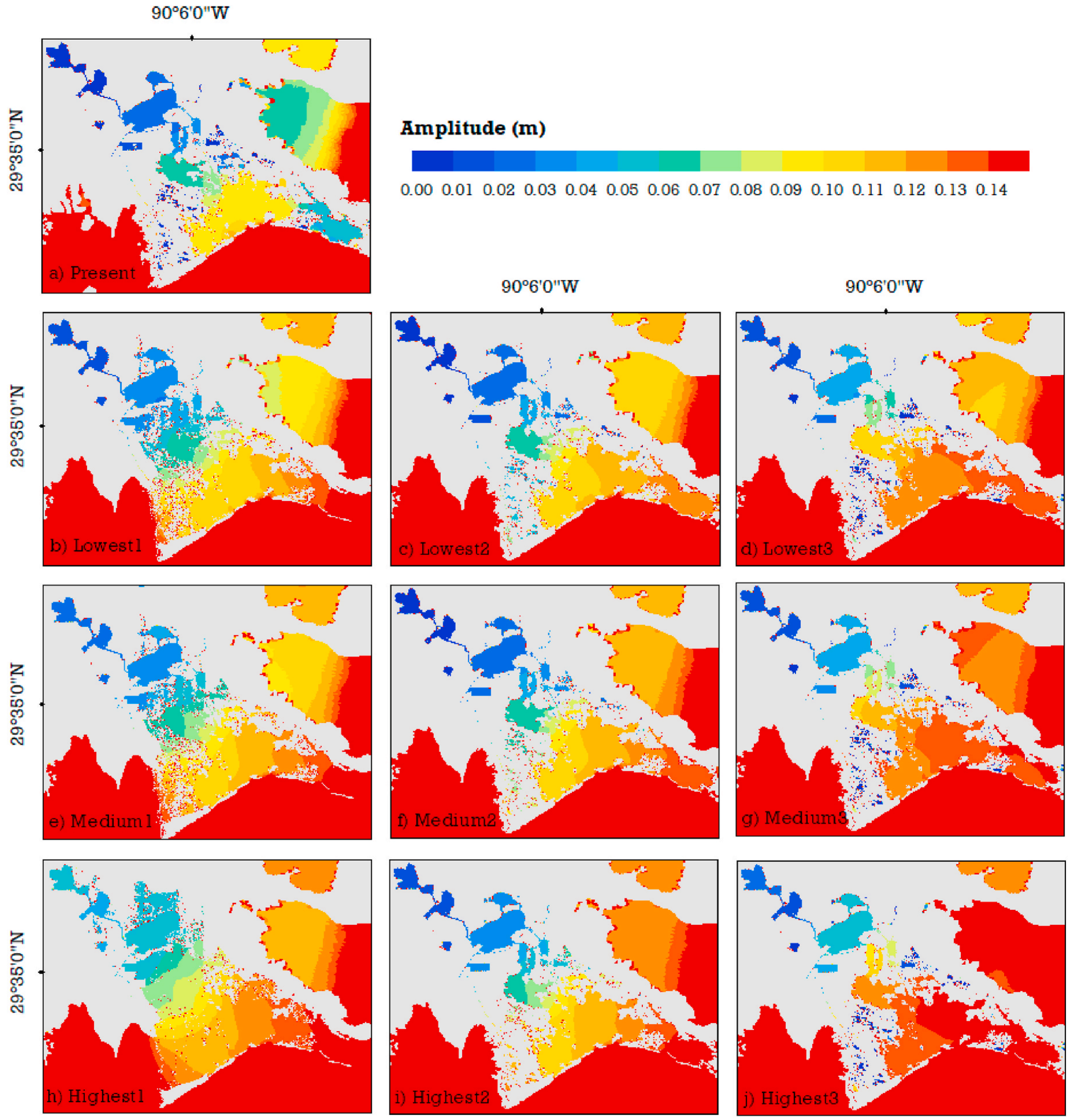

Fig. 8. K1 amplitudes under the present-day sea level conditions and for various future RSLR scenarios.

Simulation results demonstrated amplification of tides at the head of the estuary. This amplification was absent under the present-day condition and highest under the Highest1 scenario (Fig. 7g). Under the Highest1 scenario, tidal range reached a minimum at the middle of the Bayou des Allemands, approximately 92 km from the estuary's mouth, and was amplified substantially (5 cm) at the head of estuary. This amplification can also be seen in K1 amplitudes (Figs. 7 and 8). Importantly, MTR difference was positive for all scenarios, suggesting that the RSLR only increased the tidal range in Barataria Basin (Fig. 6).

7.1. Analysis of the momentum equation

To further investigate how forcing mechanisms change under the higher sea levels, a momentum balance analysis was done using the vertically averaged momentum equations with constant density (Chen et al., 2013):

$$\frac{1}{D}\frac{\partial \bar{U}D}{\partial t} = -\frac{1}{D}\left(\frac{\partial \overline{U\ UD}}{\partial x} + \frac{\partial \overline{U\ VD}}{\partial y}\right) + f\,\bar{V} - g\frac{\partial \varsigma}{\partial x} - \frac{\tau_{bx}}{D_{\rho_0}} + \tilde{F}_x + \frac{1}{D}G_x \tag{3}$$

$$\underbrace{\frac{1}{D}\frac{\partial \bar{V}D}{\partial t}}_{\text{DDT}} = \underbrace{-\frac{1}{D}\left(\frac{\partial \overline{U\ VD}}{\partial x} + \frac{\partial \overline{V\ VD}}{\partial y}\right)}_{\text{ADV}} \underbrace{-f\,\bar{U}}_{\text{COR}} \underbrace{-g\frac{\partial \varsigma}{\partial y}}_{\text{DP}} \underbrace{-\frac{\tau_{by}}{D_{\rho_0}}}_{\text{FRIC}} \underbrace{+\tilde{F}_y}_{\text{VIS}} \underbrace{+\frac{1}{D}G_y}_{\text{AD2D}} \tag{4}$$

where all variables are conventional, and the overbars denote the vertical integration. The terms from left to right in Equations (3) and (4) are local acceleration (DDT), nonlinear advection (ADV), Coriolis force (COR), barotropic pressure gradient (DP), bottom friction (FRIC), 2-D horizontal viscosity (VIS), and the difference between nonlinear terms of vertically averaged 2-D variables and vertical integration of 3-D variables (AV2D). The expressions for $\tilde{F}_x$, $\tilde{F}_y$, G_x and G_y can be found in Chen et al. (2013).

Time series of the various terms in Equations (3) and (4) for three

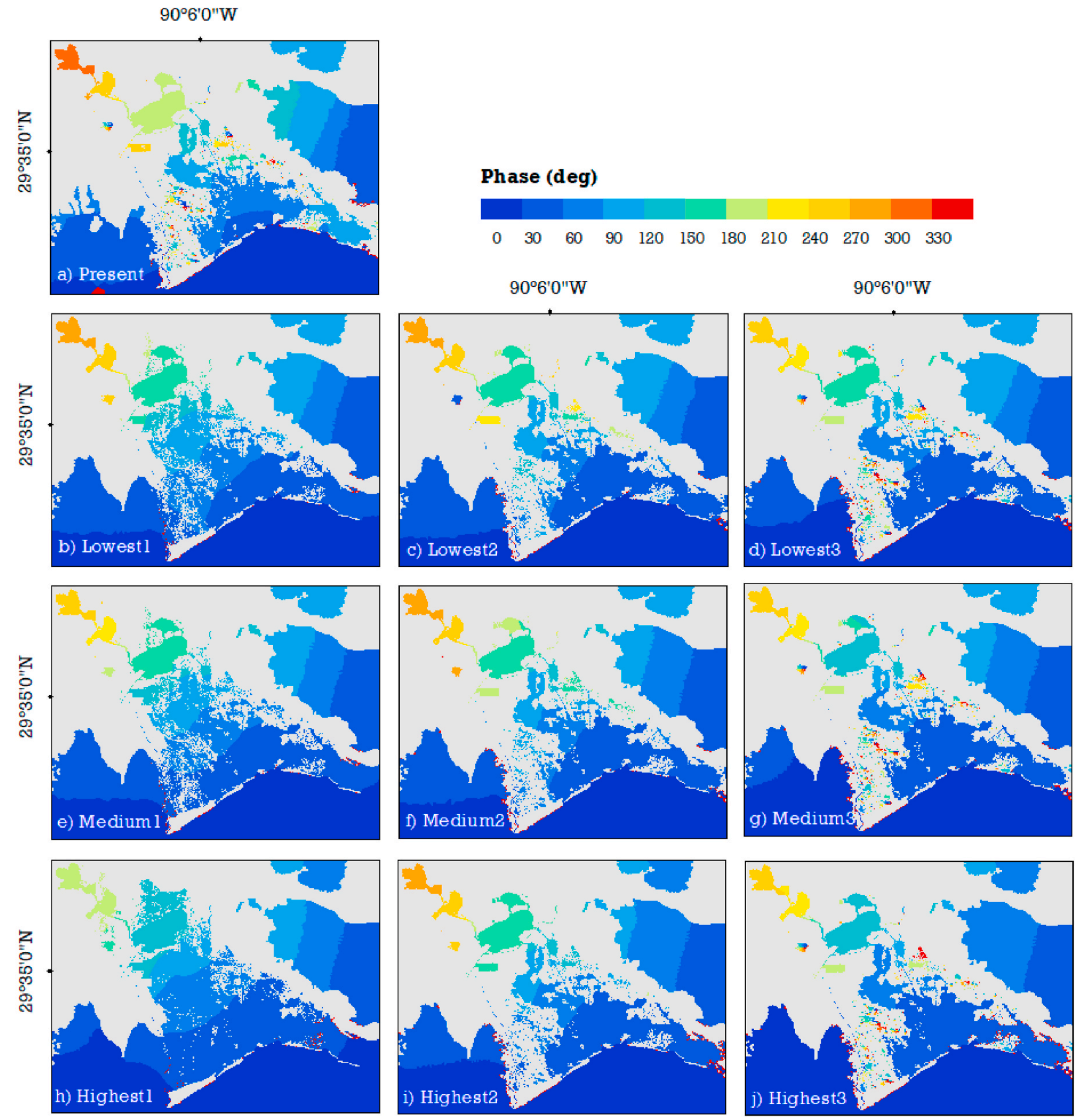

Fig. 9. K_1 phase under the present-day sea level conditions for various future RSLR scenarios.

stations located at the mouth (M1), in the middle (M2), and in the upper estuary (M3) and for three scenarios of Highest1, Highest2 and Highest3 are shown in Figs. 10 and 11 (see Fig. 1 for station locations).

Under the present-day sea level condition, for station M1 in Barataria Pass (station M1), the maximum value of positive u (1.07 m s^{-1}) was greater than the maximum negative u (0.78 m s^{-1}). Also, the maximum value of positive v (0.81 m s^{-1}) was greater than the maximum negative value of v (0.71 m s^{-1}) (Figs. 10a and 11a). This suggests that tidal velocity was asymmetric in Barataria Pass. Under the Highest1 scenario, both positive and negative u velocities increased in magnitude, but the v velocity remained unchanged. The maximum positive u increased to 1.18 m s^{-1} and maximum negative u increased to 0.93 m s^{-1} (Figs. 10b and 11b). Both velocities remained unchanged under the Highest2 scenario (Figs. 10c and 11c). However, for the Highest3 scenario, the u and v velocities were very close to their present-day values (Figs. 10d and 11d). Thus, it appears that the asymmetric nature of the currents was not altered by RSLR although their intensity decreased in the Highest1 scenario. The main momentum balance at station M1 was between DP and ADV. This was true for both flood and ebb cycles and for all RSLR scenarios. This is consistent with the previous study of Cui et al. (2018) who also reported the same balance between DP and ADV in Barataria Pass using a three-dimensional baroclinic FVCOM model. The above indicates that the tidal phenomenon at this location (depth ~20 m) is dominated by wave dynamics, as pointed out by Huang et al. (2011) and Cui et al. (2018). Both DP and ADV increase in magnitude as sea level rises while the balance between them remains unchanged.

Under the present sea level conditions, the u velocity in the mid-estuary region (station M2) was greater than the v velocity. Station M2 is located in a bayou oriented mainly in an east-west direction (Figs. 10e and 11e). The depth at this station is ~2.8 m. As sea level increased, the maximum u velocity decreased from 0.36 m s^{-1} in the present-day scenario to 0.15 m s^{-1} in the Highest1 and 0.26 m s^{-1} in the Highest2 scenarios. It increased again to 0.36 m s^{-1} under the Highest3 scenario (Fig. 10e, f, 10g, 10h). The u velocity was the smallest in the Highest1 scenario because the highest flooding extent occurred under this condition and subsequently produced the strongest frictional effects

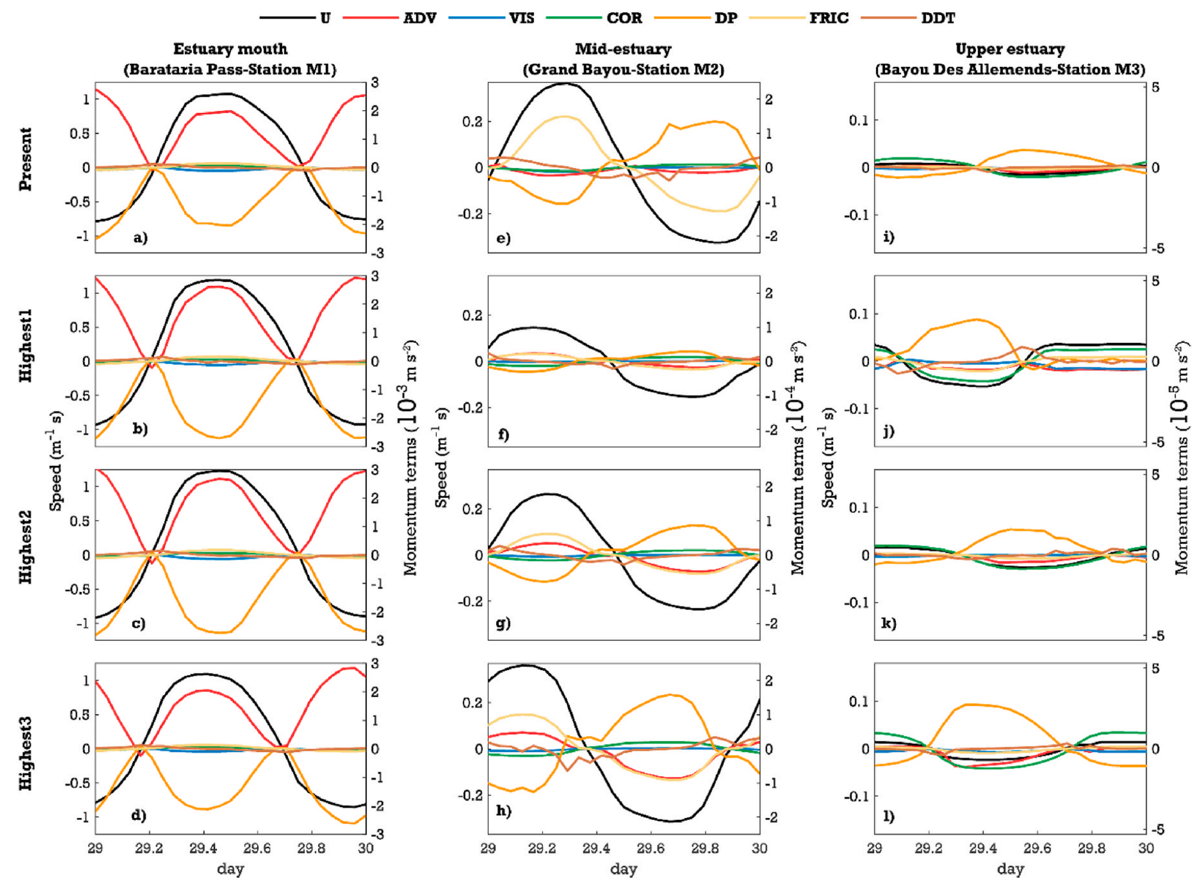

Fig. 10. Time series of vertically averaged momentum equation terms in x direction at stations M1, M2 and M3 (Fig. 1) for the present-day sea level condition and Highest1, Highest2, and Highest3 RSLR scenarios. DDT represents the local acceleration, FRIC the bottom friction, DP the barotropic pressure gradient, COR the Coriolis force, VIS the horizontal viscosity, and ADV the nonlinear advection. U is x velocity component, which characterizes the tidal cycle.

(Fig. 5 and Table 3). Under the Highest3 simulation where marsh was accreted at 100% of RSLR, the u and v magnitudes were close to the present-day conditions but with 2.9 h phase lead, which indicates that tidal waves propagated faster in the Highest3 scenario compared to the present-day condition. This occurred because RSLR deepened the channels and bayous and consequently increased the conveyance effects of the estuary. Under the present-day conditions, the main x-momentum balance at station M2 during both ebb and flood phases was due to DP and FRIC. This is consistent with previous studies suggesting that in frictionally dominated estuaries the lowest order dynamics is characterized by a zero-inertia equation, i.e., balance between bottom friction and pressure gradient (LeBlond, 1978; Friedrichs and Madsen, 1992; Huang et al., 2011). Consequently, for the present sea level, tidal wave propagation at this location can be described as a diffusion rather than a wave propagation (LeBlond, 1978). As sea level increased, the contribution of both FRIC and DP decreased and the importance of ADV and DDT increased, and thus tides became more propagational in nature (Fig. 10e, f, 10g, 10h).

For the upper estuary station M3, under the present-day sea levels the v velocity was greater than the u velocity. Station M3 is located in Bayou des Allemands which is oriented mainly in a north-south direction (Figs. 10i and 11i). The v velocity was symmetric with equal maximum positive and negative values (0.08 m s^{-1}). As sea level increased, positive and negative v velocities also increased. Under the Highest1 scenario, the maximum positive and negative v were 0.17 m s^{-1} and 0.10 m s^{-1}, respectively. This indicates that the flow in Bayou des Allemands was flood dominated in the Highest1 scenario, but the ebb flow (negative v) retained its maximum value (0.10 m s^{-1}) for most of the ebb cycle (~10 h). The momentum balance for M3 station was more complex than other stations. Under the present-day sea level conditions, the main y-momentum balance was among ADV, DP and FRIC. As sea level increased, the contribution of ADV and DDT increased, suggesting that the tide became increasingly a wave phenomenon rather than diffusion of a tidal signal. Comparing the tidal phases at different stations suggested that at the estuary mouth tidal phase does not change much with sea level rise, while in the middle and upper estuary sea level variations have a stronger influence on the tidal phase. This feature was also shown before for individual K_1 phases (Fig. 7).

8. Discussions

Model simulations showed substantial tidal choking that occurs throughout the estuary. This is consistent with previous findings of Howes (2007). Results suggest that tidal range in Barataria bay will increase for all scenarios of sea level rise and marsh vertical accretion that we have examined (Figs. 6 and 7). This is contrary to several previous studies that reported that if low-lying estuarine areas are inundated in response to sea level rise, tidal range would decrease. For example, Lee et al. (2017) found that tidal range decreases in both Chesapeake Bay and Delaware Bay when low-lying land is allowed to become permanently inundated by higher sea level. Holleman and Stacey (2014) found a similar result in a modeling study of San Francisco Bay. In those estuaries which are much deeper than Barataria Bay, when low-lying land is allowed to flood, increased dissipation in newly inundated areas offsets reduced dissipation in deeper water and therefore causes an overall reduction in the tidal range (Lee et al., 2017; Holleman and Stacey, 2014; Pelling and Green, 2013). In contrast, our modeling results indicated that even in the Highest1 scenario when no accretion was applied and extensive low-lying lands were flooded, tidal

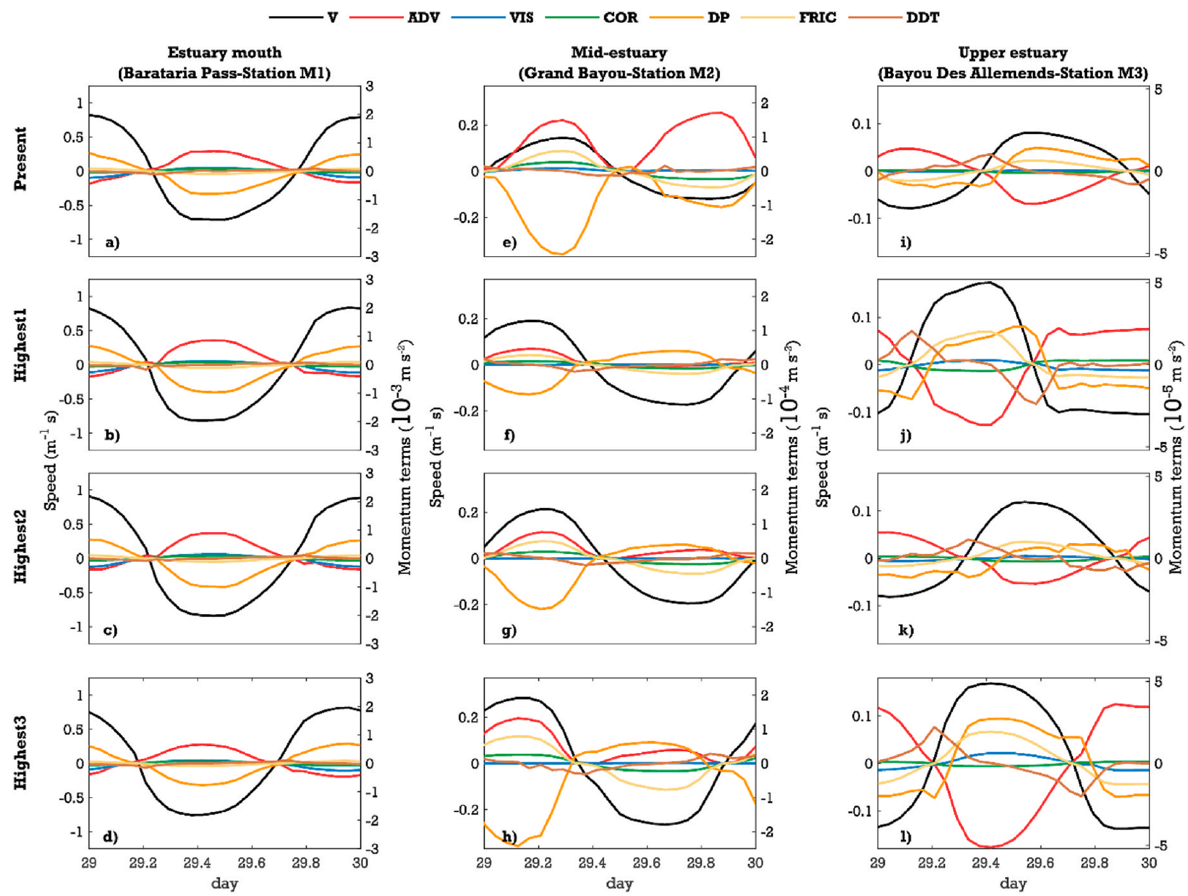

Fig. 11. Same as Fig. 10 except in y direction.

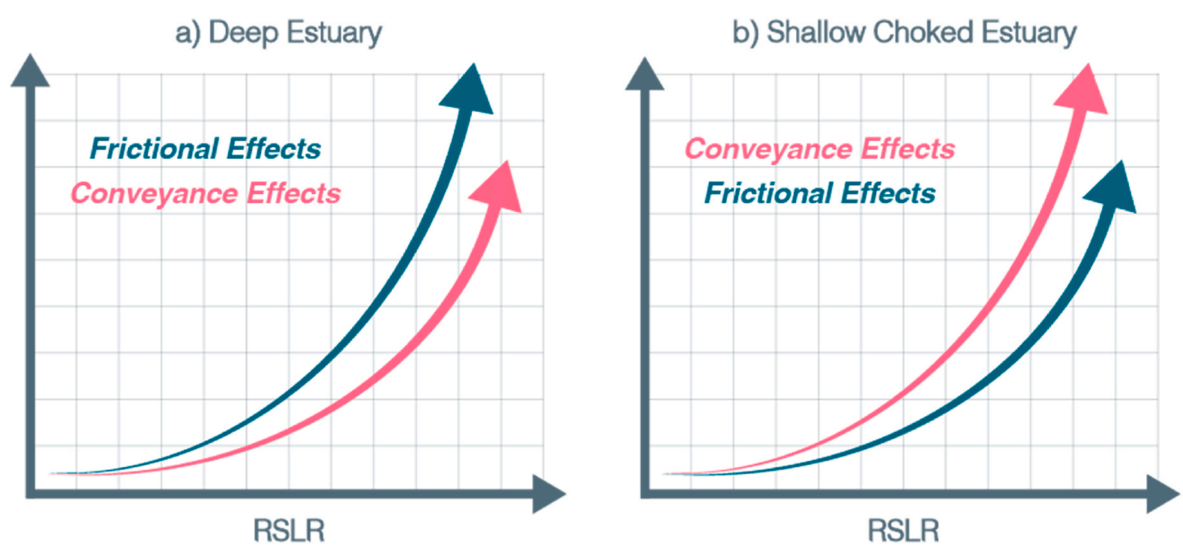

Fig. 12. Conceptual plot showing the estuary response to RSLR in a) deep Estuary, and b) shallow choked estuary.

range increased all over the bay. A Conceptual plot showing the estuary response to RSLR in a deep Estuary, and a shallow choked estuary is shown in Fig. 12. Generally, RSLR increases the frictional effects by flooding of the low-lying lands and at the same time increases the conveyance effects through deepening of the existing channels and enhancing water exchange through newly flooded areas. However, if the estuary is deep, increased conveyance effect may be smaller or negligible compared to the increased frictional effect (Fig. 12a). In contrast, if the estuary is shallow like Barataria Bay, increased conveyance effect maybe larger than increased frictional effect (Fig. 12b). This is why model predicts an increase in tidal range within Barataria Bay even when extensive wetland areas are flooded. Increased conveyance effects can also be inferred from K_1 phase differences between the mouth and the head of the estuary, suggesting that tidal waves traveled faster under future RSLR scenarios compared to the present-day sea level conditions (Table 3).

The above reasoning can also explain why in the lower and middle Barataria bay, the largest increase in tidal range occurred when the marsh area was assumed to keep pace with RSLR (less inundation). However, in the upper bay the largest increase in tidal range occurred when no accretion was assumed (higher inundation). This is because the lower and the middle bay are relatively deeper, and they have higher water exchange with the coastal ocean. In contrast, the upper bay is shallower and the openings to interior bayous and lakes are choked by constricted channels. In the upper bay, the channel conveyance effect is larger than the frictional effect of the low-lying areas. Generally, tidal range dynamics in a channel-wetland-marsh complex is mainly controlled by bottom friction. RSLR increases the frictional effect of the newly inundated low-lying marsh that cause reduction in tidal range, while, at the same time, decreases the tidal retardation in relatively deep channels due to increased water depth, reduced bottom friction, and consequent tidal range increase. Therefore, flooding of the low-lying lands in the lower bay increases the frictional effects more than conveyance effects (Fig. 12a) however in the upper bay, flooding of the low-lying lands increases the conveyance effects more than frictional effects (Fig. 12b). Comparing the K_1 phase difference between the mouth and the head of the estuary in different scenarios confirms this reasoning as it indicates that tidal waves appear to travel faster under scenarios where no accretion is assumed (Table 3). It also explains why tidal amplification in the upper bay only occurred under the Lowest1, Medium1 and Highest1 scenarios (Figs. 6, 7g and 7h). Tidal amplification is also reported in the modeling studies of tides on other estuaries. For example, Lee et al. (2017) demonstrated that sea level rise induced tidal amplification in the upper part of Chesapeake Bay and Delaware Bay. Van Rijn (2011) found that in sufficiently long, deep, and converging estuaries, the amplifying effects dominate, and tidal amplitude increases toward the head of the estuary. Holleman and Stacey (2014) demonstrated that increased mean sea level, while preserving original shorelines, produces additional tidal amplification in San Francisco Bay. A detailed momentum balance analysis in this study suggested that sea level rise shifts tidal dynamics in Barataria Bay from a dissipative tidal regime to a progressive wave which is more susceptible to tidal amplification (Figs. 10 and 11).

8.1. Limitation of the analysis

This research further demonstrates the importance of moving beyond bathtub modeling approaches by shifting the paradigm of RSLR assessments to approaches that account for the coastal dynamics of sea level rise (Passeri et al., 2015b). By more completely representing and examining the physiographic characteristics and future sea level trends of the estuarine system we have further distinguished the nonlinearity of RSLR. However, predictions of this study still have limitations. Examples of such limitations include the accretion of the channels and bay bottom which were not considered. Even in simulations where the marshes were assumed to accrete at the same rate of RSLR, the bottom did not have any accretion. However, in reality the bottom of the estuary can accrete if some sediment is imported into Barataria Bay, for example from the coastal ocean (Payandeh et al., 2020), from the GIWW (Mariotti et al., 2021), or from the David Pond diversion (Keogh et al., 2019). Furthermore, the model did not account for changes in marsh extent. Lateral retreat of the marshes can widen the channels, and thus affect tidal propagation. A reduction in marsh area is expected to increase tidal range. Similarly, the model did not include changes in barrier islands or tidal inlets. Barrier fragmentation and inlet widening, and deepening will likely increase conveyance and thus tidal range. Both changes in marsh area and barrier morphology is difficult to predict, especially since it is strongly dependent on human actions (i.e., coastal restoration). Finally, uncertainties associated with digital elevation models (DEMs) could affect the present-day inundations predicted by the model and also the future tidal responses. A higher resolution and more accurate bathymetry data for the shallow regions of the northern Gulf of Mexico would benefit the future modeling efforts.

9. Conclusion

This study quantified the combined effects of RSLR and marsh accretion on tidal dynamics in a tidally choked estuary. Under the present-day sea level conditions, five major tidal choking areas were identified within Barataria Bay where tidal ranges were reduced sharply and phase lags occurred. RSLR reduced tidal choking intensity and thus increased tidal range within the estuary. Despite the previous modeling studies in other estuaries suggesting that flooding of the low-lying areas in response to sea level rise would increase tidal dissipation and thus reduce tidal ranges, our study suggests that in a choked tidal system such as Barataria Bay the tidal range is likely to increase even when extensive wetland areas are flooded. This is because the channel conveyance effect is larger than the frictional effect of the low-lying areas. The most interesting result of this study is that the change in tidal range varies along the estuary axis, and it is strongly dependent on the marsh vertical accretion. In the lower and the middle estuary, the largest increase in tidal range (up to 16 cm) occurred when the marsh area was assumed to keep pace with RSLR. In the upper estuary, the largest increase in tidal range (up to 13 cm) occurred when no accretion was assumed. RSLR also induced amplification of tides at the head of the estuary. A detailed momentum balance analysis indicated that sea level rise shifts tidal regime from a dissipative tidal wave to a progressive wave which is more susceptible to tidal amplification. The positive feedback between RSLR and higher tidal ranges contributes to rapidly increasing inundation in the future. Under a less optimistic scenario, it was predicted that 75% of the model domain in Barataria Bay will be permanently flooded while the remaining 25% will be partially flooded. Given that inundations reported in this study are only tidally induced, the actual inundations would be larger if subtidal water levels were added to the RSLR models. While this study focused only on the impacts of RSLR and marsh accretion on tidal dynamics, it is important to note that other changes in the geomorphology, such as changes in the bay bottom, the lateral marsh extent, and the barrier islands erosion, could also occur in the future. Therefore, additional research is needed to investigate the combined effects of future RSLR and geomorphology changes on tidal dynamics in Barataria Bay.

Declaration of competing interest

The authors declare that they have no known competing financial interests or personal relationships that could have appeared to influence the work reported in this paper.

Acknowledgement

This research was made possible in part by a grant from The Gulf of Mexico Research Initiative. Data are publicly available through the Gulf of Mexico Research Initiative Information and Data Cooperative (GRIIDC) at https://data.gulfresearchinitiative.org (DOI: 10.7266/n7-s2q1-5521). A. R. Payandeh was also supported in part by the Economic Development Assistantship from the Graduate School, Louisiana State University.

References

Bilskie, M.V., Hagen, S.C., Medeiros, S.C., Passeri, D.L., 2014. Dynamics of sea level rise and coastal flooding on a changing landscape. Geophys. Res. Lett. 41 (3) https://doi.org/10.1002/2013GL058759, 927–234.

Blum, M.D., Tomkin, J.H., Purcell, A., Lancaster, R.R., 2008. Ups and downs of the Mississippi delta. Geology 36, 675–678.

Bunya, S., et al., 2010. A high-resolution coupled riverine flow, tide, wind, wind wave, and storm surge model for southeastern Louisiana and Mississippi. Part I: model development and validation. Mon. Weather Rev. 128, 345–377.

Byrne, P., Borengasser, M., Drew, G., Muller, R.A., Smith, J., Wax, C., 1976. Barataria Bay: Hydrologic and Climatologic Processes. Louisiana State University Center for Wetland Resources: Sea Grant Publ. No. LSU-T-76-010.
Chen, C., Beardsley, R.C., Cowles, G., 2013. An Unstructured Grid, Finite-Volume Coastal Ocean Model: FVCOM User Manual. School for Marine Science and Technology, University of Massachusetts Dartmouth, p. 315.
Chen, C., Liu, H., Beardsley, R.C., 2003. An unstructured grid, finite-volume, three dimensional, primitive equations ocean model: application to coastal ocean and estuaries. J. Atmos. Ocean. Technol. 20, 159e186.
Coastal Protection and Restoration Authority (CPRA), 2012. *Louisiana's Comprehensive Master Plan for a Sustainable Coast*. State of Louisiana. Baton Rouge (LA). Retrieved from. http://www.coastalmasterplan.la.gov/.
The ecology of Barataria Bay, Louisiana: An estuarine profile (165 pp. National Wetlands Research Center, U.S. Fish Wildlife Service. In: Conner, W.H., Day, J.W., Pendleton, E.C. (Eds.), Biol. Rep. (Wash. D C) 85 (7), 13.
Couvillion, B.R., Beck, H., Schoolmaster, D., Fischer, M., 2017. Land Area Change in Coastal Louisiana (1932 to 2016). Technical Report Scientific Investigations Map, U. S. Geological Survey, Reston. https://doi.org/10.3133/sim3381.
Cui, L., Huang, H., Li, C., Justic, D., 2018. Lateral circulation in a partially stratified tidal inlet. J. Mar. Sci. Eng. 6 (4), 159–181. https://doi.org/10.3390/jmse6040159.
Day Jr., J.W., Boesch, D.F., Clairain, E.J., Kemp, G.P., Laska, S.B., Mitsch, W.J., Orth, K., Mashriqui, H., Reed, D.J., Shabman, L., Simenstad, C.A., Streever, B.J., Twilley, R.R., Watson, C.C., Wells, J.T., Whigham, D.F., 2007. Restoration of the Mississippi delta: lessons from hurricanes Katrina and Rita. Science 315 (5819), 1679–1684. https://doi.org/10.1126/science.1137030.
Day Jr., J.W., Britsch, L.D., Hawes, S.R., Shaffer, G.P., Reed, D.J., Cahoon, D., 2000. Pattern and process of land loss in the Mississippi delta: a spatial and temporal analysis of wetland habitat change. Estuaries 23 (4), 425–438. https://doi.org/10.2307/1353136.
Du, J., Shen, J., Zhang, Y.J., Ye, F., Liu, Z., Wang, Z., et al., 2018. Tidal response to sea-level rise in different types of estuaries: the importance of length, bathymetry, and geometry. Geophys. Res. Lett. 45, 227–235. https://doi.org/10.1002/2017GL075963.
FitzGerald, D.M., Hein, C.J., Connell, J.E., Hughes, Z.J., Georgiou, I.Y., Novak, A.B., 2021. Largest marsh in New England near a precipice. Geomorphology. https://doi.org/10.1016/j.geomorph.2021.107625, 107625.
Friedrichs, C.T., Madsen, O.S., 1992. Non-linear diffusion of the tidal signal in frictionally dominated embayments. J. Geophys. Res. 97, 5637e5650.
Friedrichs, C.T., Perry, J.E., 2001. Tidal salt marsh morphodynamics: a synthesis. J. Coast Res. 27, 7–37.
Hagen, S.C., Bacopoulos, P., 2012. Coastal flooding in Florida's big bend region with application to sea level rise based on synthetic storms analysis. Terr. Atmos. Ocean Sci. 23 (No. 5), 481–500. https://doi.org/10.3319/TAO.2012.04.17.01(WMH. October 2012.
Hiatt, M., Snedden, G., Day, J.W., Rohli, R.V., Nyman, J.A., Lane, R., Sharp, L.A., 2019. Driversand impacts of water levelfluctuations in the Mississippi River delta: implications fordelta restoration. Estuar. Coast Shelf Sci. 224, 117–137.
Holleman, R.C., Stacey, M.T., 2014. Coupling of sea level rise, tidal amplification, and inundation. J. Phys. Oceanogr. 44 (5), 1439–1455. https://doi.org/10.1175/JPO-D-13-0214.1.
Howes, N.C., 2007. The Impact of Wetland Loss on Inlet Morphology and Tidal Range within Barataria Bay, Louisiana: MS. Thesis, University of Boston, Boston, Massachusetts, p. 107.
Huang, H., Justic, D., Lane, R.R., Day, J.W., Cable, J.E., 2011. Hydrodynamic response of the Breton Sound estuary to pulsed Mississippi River inputs. Estuar. Coast Shelf Sci. 95 (1), 216–231. https://doi.org/10.1016/j.ecss.2011.08.034.
Huang, W., Li, C., 2017. Cold front driven flows through multiple inlets of Lake Pontchartrain Estuary. J. Geophys. Res.: Oceans 122, 8627–8645. https://doi.org/10.1002/2017JC012977.
Keogh, M.E., Alexander, S., Kolker, A.S., Snedden, G.A., Renfro, A.A., 2019. Hydrodynamic controls on sediment retention in an emerging diversion-fed delta. Geomorphology 332, 100–111. https://doi.org/10.1016/j.geomorph.2019.02.008, 2019.
Kirwan, M.L., Brad Murray, A., 2007. A coupled geomorphic and ecological model of tidal marsh evolution. Proceedings of the National Academy of Sciences Apr 104 (15), 6118–6122. https://doi.org/10.1073/pnas.0700958104, 2007.
LeBlond, P.H., 1978. On tidal propagation in shallow rivers. J. Geophys. Res. 83, 4717e4721.
Lee, S.B., Li, M., Zhang, F., 2017. Impact of sea level rise on tidal range in Chesapeake and Delaware Bays. J. Geophys. Res.: Oceans 122, 3917–3938. https://doi.org/10.1002/2016JC012597.
Li, C., White, J.R., Chen, C., Lin, H., Weeks, E., Galvan, K., Bargu, S., 2011. Summertime tidal flushing of Barataria Bay: transports of water and suspended sediments. J. Geophys. Res. 116, C04009. https://doi.org/10.1029/2010JC006566.
Mariotti, G., Fagherazzi, S., 2010. A numerical model for the coupled long-term evolution of salt marshes and tidal flats. J. Geophys. Res. 115, F01004. https://doi.org/10.1029/2009JF001326.
Mariotti, G., Ceccherini, G., McDonell, M., et al., 2021. A Comprehensive Assessment of Sediment Dynamics in the Barataria Bay (LA, USA) Distinguishes Riverine Advection from Wave Resuspension and Identifies the Gulf Intracoastal Waterway as a Major Sediment Source. *Estuaries And Coasts*. https://doi.org/10.1007/s12237-021-00957-8.
Monsen, N.E., Cloern, J.E., Lucas, L.V., Monismith, S.G., 2002. The use of flushing time, residence time, and age as transport time scales. Limnol. Oceanogr. 47 (5), 1545–1553. https://doi.org/10.4319/lo.2002.47.5.1545.
Orson, R., Panageotou, W., Leatherman, S.P., 1985. Response of tidal salt marshes of the U.S. Atlantic and Gulf Coasts to rising sea levels. J. Coast Res. 1, 29–37.
Paola, C., Twilley, R.R., Edmonds, D.A., Kim, W., Mohrig, D., Parker, G., Viparelli, E., Voller, V.R., 2011. Natural processes in delta restoration: application to the Mississippi Delta. Ann. Rev. Mar. Sci 3, 67–91. https://doi.org/10.1146/annurevmarine- 120709-142856.
Passeri, D.L., Hagen, S.C., Plant, N.G., Bilskie, M.V., Medeiros, S.C., Alizad, K., 2016. Tidal hydrodynamics under future sea level rise and coastal morphology in the Northern Gulf of Mexico. Earth's Future 4, 159–176. https://doi.org/10.1002/2015EF000332.
Passeri, D.L., Hagen, S.C., Medeiros, S.C., Bilskie, M.V., 2015a. Impacts of historic morphology and sea level rise on tidal hydrodynamics in a microtidal estuary (Grand Bay, Mississippi). Continent. Shelf Res. 111, 150–158. https://doi.org/10.1016/j.csr.2015.08.001.
Passeri, D.L., Hagen, S.C., Medeiros, S.C., Bilskie, M.V., Alizad, K., Wang, D., 2015b. The dynamic effects of sea level rise on low-gradient coastal landscapes: a review. Earth's Future 3, 159–181. https://doi.org/10.1002/2015EF000298.
Pasternack, G.B., Hilgartner, W.B., Brush, G.S., 2000. Biogeomorphology of an upper Chesapeake Bay river-mouth tidal freshwater marsh. Wetlands 20, 520–537. https://doi.org/10.1672/0277-5212(2000)020<0520:BOAUCB>2.0.CO;2.
Payandeh, A.R., Justic, D., Mariotti, G., Huang, H., Sorourian, S., 2019. Subtidal water level and current variability in a bar-built estuary during cold front season: Barataria Bay, Gulf of Mexico. J. Geophys. Res.: Oceans 124, 7226–7246. https://doi.org/10.1029/2019JC015081.
Payandeh, A.R., Justic, D., Mariotti, G., Huang, H., Valentine, K., 2020. Suspended sediment dynamics in a deltaic estuary controlled by subtidal motion and offshore river plumes. Journal of Estuarine, Coastal and Shelf Sciences. https://doi.org/10.1016/j.ecss.2020.107137.
Pelling, H.E., Green, J.A.M., 2013. Sea level rise and tidal power plants in the Gulf of Maine. J. Geophys. Res.: Oceans 118, 2863–2873. https://doi.org/10.1002/jgrc.20221.
Pickering, M.D., Horsburgh, K.J., Blundell, J.R., Hirschi, J.J.M., Nicholls, R.J., Verlaan, M., Wells, N.C., 2017. The impact of future sea-level rise on the global tides. Continent. Shelf Res. 142, 50–68. https://doi.org/10.1016/j.csr.2017.02.004.
Pickering, M.D., Wells, N.C., Horsburgh, K.J., Green, J.A.M., 2012. The impact of future sea-level rise on the European Shelf tides. Continent. Shelf Res. 35, 1–15. https://doi.org/10.1016/j.csr.2011.11.011.
Redfield, A.C., 1972. Development of a New England salt marsh. Ecol. Monogr. 42, 201–237. https://doi.org/10.2307/1942263.
Reed, D.J., 1995. The response of coastal marshes to sea-level rise: survival or submergence? Earth Surf. Process. Landforms 20, 39–48. https://doi.org/10.1002/esp.3290200105.
Siverd, C.G., Hagen, S.C., Bilskie, M.V., Braud, D.H., Peele, R.H., Foster-Martinez, M.R., Twilley, R.R., 2019. Coastal Louisiana landscape and storm surge evolution: 1850-2110. Climatic Change 157 (3–4), 445–468. https://doi.org/10.1007/s10584-019-02575-7.
Szpilka, C., Dresback, K., Kolar, R., Feyen, J., Wang, J., 2016. Improvements for the western north atlantic, caribbean and Gulf of Mexico ADCIRC tidal database (EC2015). J. Mar. Sci. Eng. 4, 1–55. https://doi.org/10.3390/jmse4040072.
Talke, S.A., Jay, D.A., 2020. Changing tides: the role of natural and anthropogenic factors. Ann. Rev. Mar. Sci 12, 14. https://doi.org/10.1146/annurev-marine-010419-010727, 1–14.31.
Thomson, R.E., Emery, W.J., 2014. Data Analysis Methods in Physical Oceanography, third ed. Elsevier, Amsterdam, Netherlands.
Torres, R., Fagherazzi, S., van Proosdij, D., Hopkinson, C., 2006. Salt marsh geomorphology: physical and ecological effects on landform. Estuar. Coast Shelf Sci. 69, 309–310. https://doi.org/10.1016/j.ecss.2006.05.001.
Van Rijn, L.C., 2011. Analytical and numerical analysis of tides and salinities in estuaries; Part I: tidal wave propagation in convergent estuaries. Ocean Dynam. 61, 1719–1741. https://doi.org/10.1007/s10236-011-0453-0.
Veatch, W., 2015. Updated Atlas of U.S. Army Corps of Engineers Historic Daily Tide Data in Coastal Louisiana. MRG&P Report. No. 14 • November 2017.
Wang, L., Justic, D., 2009. A modeling study of the physical processes affecting the development of seasonal hypoxia over the inner Louisiana-Texas shelf: circulation and stratification. Continent. Shelf Res. 29 (11-12), 1464–1476. https://doi.org/10.1016/j.csr.2009.03.014.
Zhang, K., 2011. Analysis of non-linear inundation for sea-level rise using LIDAR data: a case study for South Florida. Clim. Change 106, 537–565.
Shrull, S. Bryant. (2018), Spatial Trends and Variability of Marsh Accretion Rates in Barataria Basin, Louisiana, USA Using 210Pb and 137Cs Radiochemistry. LSU Master's Theses. 4751.